DOI: 10.1002/((please add manuscript number))
Article type: Full Paper

Band edge engineering of oxide photoanodes for photoelectrochemical water splitting: Integration of subsurface dipoles with atomic-scale control

Yasuyuki Hikita, Kazunori Nishio, Linsey C. Seitz, Pongkarn Chakthranont, Takashi Tachikawa, Thomas F. Jaramillo, Harold Y. Hwang*

Dr. Yasuyuki Hikita, Dr. Kazunori Nishio, Dr. Takashi Tachikawa, Prof. Harold Y. Hwang
Stanford Institute for Materials and Energy Sciences, SLAC National Accelerator Laboratory
2575 Sand Hill Road, Menlo Park, California, 94025, USA.
E-mail: hikita@stanford.edu

Dr. Linsey C. Seitz, Pongkarn Chakthranont, Prof. Thomas F. Jaramillo
Department of Chemical Engineering, Stanford University
Shriram Center, 443 Via Ortega, Stanford, California, 94305, USA.

Prof. Thomas F. Jaramillo
SUNCAT Center for Interface Science and Catalysis, SLAC National Accelerator Laboratory
2575 Sand Hill Road, Menlo Park, California, 94025, USA.

Dr. Kazunori Nishio and Prof. Harold Y. Hwang
Geballe Laboratory for Advanced Materials, Department of Applied Physics, Stanford University
476 Lomita Mall, Stanford University, Stanford, California, 94305, USA.

Keywords: interface dipoles, oxide/electrolyte interfaces, photoelectrochemical cells, solar water splitting, $SrTiO_3$

Developing renewable sources of energy is one of the most important challenges in current research as global energy consumption continues to increase.[1] Hydrogen production via photoelectrochemical (PEC) water splitting is a sustainable approach to providing high energy density fuels as well as an essential feedstock for major industrial chemical synthesis.[2] Despite its potential impact as an energy conversion process utilizing abundant sources – solar irradiation and water – the efficiency of PEC water splitting remains below industrially applicable levels. The key to successful operation of PEC devices heavily relies on precise materials control and

This material is based upon work supported by the U.S. Department of Energy, Office of Science, Office of Basic Energy Sciences, Division of Materials Sciences and Engineering, under Contract No. DE-AC02-76SF00515 and NSF.

engineering of semiconductors. Recent developments in semiconductor design span a broad spectrum from exploring novel compounds to combining multi-layered heterostructures and nanostructures to maximize the solar-to-hydrogen (STH) conversion efficiency.[3,4] Among all types of semiconductors, metal oxides have shown promising attributes as photoelectrode materials for PEC devices due to their relatively high chemical stability and the flexibility to manipulate their optical and electrical properties over a wide range through their stoichiometry.[3,5]

In order to develop highly efficient oxide semiconductors, design strategies based on critical assessment of their PEC properties in well-defined forms is an effective approach. To this end, the controlled surface and bulk properties of single crystalline epitaxial thin films provide an ideal platform for investigating the intrinsic physical and electronic properties of oxides for PEC applications.[6] For example, UHV-based metal oxide thin film synthesis techniques, such as pulsed laser deposition (PLD) and molecular beam epitaxy, enable control over the defect density and thickness in ternary or even quaternary oxides on the atomic scale while preserving a well-defined surface structure,[7] suitable for evaluating the best case PEC performance for subsequent studies. Furthermore, the recent advances in thin film fabrication techniques and the conceptual breakthroughs at oxide solid-state heterointerfaces have opened new avenues to controllably introduce carriers without chemical doping and to generate built-in electric fields with atomic scale precision.[8,9] These capabilities offer the opportunity to engineer one of the most challenging elements in PEC devices – the band edge alignment at the oxide/electrolyte interface.

The band edge alignment, defined as the relative energy position of the semiconductor band edges with respect to the oxygen and hydrogen evolution potentials, critically affects the PEC performance in two ways. Firstly, it defines the thermodynamic driving force for the respective half-reaction. For example, a photoanode with a more positive valence band edge

provides larger driving force for the photo-generated holes as they oxidize water. Secondly, the flat band potential (E_{fb}) essentially governs the solar-to-electrical energy conversion efficiency through modulation of the space-charge layer thickness, which spatially separates the photo-generated electrons and holes. Previous approaches to control band edge alignment have primarily focused on the chemical functionalization of compound semiconductor surfaces by organic molecules and ions which, despite their success in non-aqueous systems,[10] generally lead to marginal tunability in aqueous solutions needed for PEC water splitting.[11] This is mainly due to the strong surface hydroxylation equilibria of oxides,[12] making band edge alignment a materials specific parameter and hence limiting the efficiency of many oxides.

This limitation can potentially be overcome by considering the electrostatics at these interfaces, which predicts that a potential difference can be generated by inserting a pair of oppositely charged species within atomic distances of the interface. The potential generated by such an interface dipole is proportional to the magnitude of the charge, which offsets the band edge alignment in the direction determined by the stacking sequence of the positive and negative charges.[13] Recently, this concept was implemented in solid-state all-oxide Schottky junctions to control their barrier heights.[14] The strong ionic bonding in metal oxides and the unique perovskite crystal structure enable natural dipole incorporation at heterointerfaces which generate a potential offset large enough to convert a rectifying Schottky junction into an Ohmic contact.[9] Here we apply this dipole engineering technique to a prototypical oxide/aqueous solution interface and demonstrate the tuning of the flat band potential over 1.3 V by inserting a ~1 nm dipole layer, significantly exceeding previous modulation of E_{fb}.[11] A crucial underlying aspect in this study is the insertion of complete dipole layers, consisting of both positive and the negative charges, at the subsurface rather than at the oxide/electrolyte interface, enabling activation and stability of the full dipole magnitude expected from the ionic charge layers.

We engineered an *n*-type 0.01 wt. % Nb-doped $SrTiO_3$ (Nb:$SrTiO_3$) photoanode by forming an ultrathin $LaAlO_3$ as the dipole layer, and capped it with a non-doped $SrTiO_3$ layer. $SrTiO_3$ is a well-studied semiconductor in PEC with a cubic perovskite structure having an optical gap of 3.2 eV,[15] and is available in high quality single crystalline form with well-defined atomically flat surfaces.[16] In the pseudocubic notation, the $LaAlO_3$ crystal structure projected in the [001] orientation consists of alternate stacking of $(AlO_2)^-$ and $(LaO)^+$ charged layers assuming nominal valence for the ions, in contrast to the charge neutral stacking of $(TiO_2)^0$ and $(SrO)^0$ in $SrTiO_3$ (**Figure 1a**). By terminating the Nb:$SrTiO_3$ (001) surface with the TiO_2 layer,[16] $LaAlO_3$ growth naturally starts from the $(LaO)^+$ layer forming a dipole potential pointing towards the Nb:$SrTiO_3$ (001) surface, equivalent to increasing the electron affinity of Nb:$SrTiO_3$. By increasing the thickness of the $LaAlO_3$ layer, the dipole potential increases up to a critical thickness, beyond which the electrostatic energy in the $LaAlO_3$ layer can no longer be stabilized and the built-in electric field gradually decreases with thickness.[17] The cap $SrTiO_3$ layer serves to avoid direct contact of $LaAlO_3$ surface to the electrolyte, preventing potential (photo)-corrosion of the dipole layer and to also maintain the same point of zero charge (PZC) regardless of the presence of the dipole layer for systematic comparison. Different chemical surfaces are expected to have different PZCs, which could result in spontaneous surface dipole formation driven by the difference in solution pH and the oxide PZC.[12,18]

A total of 12 samples were fabricated varying the $LaAlO_3$ dipole layer thickness d_{LAO} from 0 to 6 unit cells (u.c.) with a fixed 5 u.c. cap $SrTiO_3$ layer using PLD followed by a post annealing process to fill residual oxygen vacancies potentially generated during thin film growth (see Experimental Section). We note that a single unit cell corresponds to the full perovskite unit cell consisting of two atomic layers $(LaO)^+/(AlO_2)^-$ and $(SrO)^0/(TiO_2)^0$ for $LaAlO_3$ and $SrTiO_3$, respectively. The $LaAlO_3$ and $SrTiO_3$ film deposition rates were pre-calibrated by measuring the

thickness of the films deposited on $SrTiO_3$ (001) substrates at various laser pulse counts. For the $LaAlO_3$ layers, the thickness was measured by using X-ray reflectivity as shown in **Figure 1b** giving a calibrated deposition rate of 1.4×10^{-2} nm/pulse. For $SrTiO_3$, atomic force microscopy (AFM) was used for the grown film thickness measurement giving a deposition rate of 2.0×10^{-2} nm/pulse. As an independent measure of the deposition rate, reflection high-energy electron diffraction (RHEED) oscillations were taken *in situ* during deposition of these layers as shown in Supporting Information Figure S1a for a d_{LAO} = 3.0 u.c. sample. The thickness calibrations obtained from RHEED oscillations were in good agreement with those from laser pulse counts. The AFM image of a d_{LAO} = 1.0 u.c. sample in **Figure 1c** shows step-terrace surface structure, indicating an atomically flat surface after fabrication of $LaAlO_3$ (1 u.c.) and $SrTiO_3$ (5 u.c.) layers. The particle-free surface indicates that the cation stoichiometry is preserved in these layers. Similar topographies with well-defined surfaces were obtained for all 12 samples (see Supporting Information Figure S1b). The step height was 0.4 nm corresponding to a single perovskite unit cell as shown in **Figure 1d**.

We performed a Mott-Schottky analysis in 0.1 M KOH electrolyte to measure the flat band potentials of all photoelectrodes with various d_{LAO} (see Supporting Information Figure S2a for representative raw data). **Figure 2a** shows a linear $1/C^2$ - E trend in all cases at oxidizing potentials characteristic of an *n*-type semiconductor. Here, C is the capacitance deduced from the Randles model (Supporting Information Figure S2a) via electrochemical impedance measurement at each applied potential, E, measured with respect to the reversible hydrogen electrode (RHE). E_{fb} was obtained by linearly fitting the $1/C^2$ data in the anodic region against the potential. For d_{LAO} = 0 u.c., the linear fit was extrapolated to the potential axis giving E_{fb} (0 u.c.) = -0.39 V vs. RHE in agreement with previously reported values.[15] For d_{LAO} > 0 u.c., a finite residual $1/C^2$ was observed below E_{fb} which predominantly corresponds to the capacitance arising from the

$LaAlO_3$,[19] $SrTiO_3$,[20] and the electric double layers.[21] In these cases, the residual $1/C^2$ was also linearly fitted and the potential at which it intersects with the anodic slope was defined as E_{fb}. Four examples of such fitting processes are shown in **Figure 2b** for d_{LAO} = 1.0, 2.0, 3.0, and 4.0 u.c., demonstrating that a linear extrapolation to the potential axis would underestimate the E_{fb}. Thus deduced, the E_{fb} shifted anodically with increase in d_{LAO} up to 1.5 u.c. and remained almost constant above this thickness up to d_{LAO} = 6.0 u.c. (**Figure 3a**). Throughout the entire potential range, the extracted series resistance (R_u) was approximately 120 Ω and the parallel resistance (R_p) was higher than 10^7 Ω above -0.5 V vs. RHE, and exponentially decreased to 10^4 Ω under cathodic bias which confirms the negligible current leakage in the Nb:$SrTiO_3$ (001) substrates.

The cyclic voltammetry results for the initial sweep after immersing in solution under chopped illumination are shown for 9 samples in **Figure 2c**. All samples show photocurrent at high positive potentials, which diminishes under bias in the negative direction (see Supporting Information Figure S2c for measurements of all samples). The onset of the photocurrent (E_{ON}) was obtained by linearly fitting the photocurrent density J_{ph} in a $J_{ph}^2 - E$ plot close to the rise of the photocurrent and extrapolating to the potential axis as shown in Supporting Information Figure S2b. E_{ON} linearly shifts anodically up to d_{LAO} = 1.5 u.c. and also above d_{LAO} = 2.0 u.c., exhibiting a plateau in the range d_{LAO} = 1.5 to 2.0 u.c. The photocurrent density at a fixed anodic bias (E = +2.4 V vs. RHE), where saturation of the photocurrent was observed for all samples, linearly decreased with the $LaAlO_3$ thickness, due to the increasing impedance of ultrathin $LaAlO_3$ layer against hole transport. The dark current under the same bias remained substantially smaller than the photocurrent, showing a slight increase from 0.2 μA/cm^2 for d_{LAO} = 0 u.c. to 1.6 μA/cm^2 for d_{LAO} = 6 u.c. The photocurrent and the dark current overlapped for sweeps in both the positive and the negative direction except for the small difference close to E_{ON}, suggesting negligible degradation of the photoanode as a function of illumination and bias. The large shift in

E_{fb} and the associated modulation in the photocurrent clearly reveal the significant impact of the nm-thick inserted $LaAlO_3$ layers on the performance of this photoanode.

As shown in **Figure 3a**, E_{fb} linearly shifts anodically with d_{LAO} up to 1.5 u.c. and saturates above, the slope corresponding to a potential shift of 0.9 V/u.c. of $LaAlO_3$. As a control experiment, we measured the built-in potential V_{bi} of Schottky junctions between Pt-metal and the dipole engineered Nb:$SrTiO_3$ heterostructures through capacitance-voltage characteristics (Supporting Information Figure S3a and S3b). As seen from Figure 3a, a quantitatively similar trend in V_{bi} was observed, strongly supporting the active role of the $LaAlO_3$ dipole layer embedded in the photoanode. Furthermore, direct measurement of the Schottky barrier height from internal photoemission (Φ_{IPE}) reveals that the Pt/cap-$SrTiO_3$ barrier height remains constant independent of d_{LAO}, supporting the validity of this model (see Supporting Information Figure S3c).[22] A schematic evolution of E_{fb} and the dipole potential is depicted in a band diagram in **Figure 3c**. The electric field inside the $LaAlO_3$ is constant up to d_{LAO} = 1.5 u.c., shown by the red lines, and decreases systematically with d_{LAO} above, shown by the light blue line in d_{LAO} = 3.0 u.c. We note that the saturating E_{fb} value above d_{LAO} = 1.5 u.c. corresponds to the oxygen evolution reaction (OER) potential (E_{OER} = +1.23 V vs. RHE) which sets the anodic boundary for the Fermi level of the system, as expected. Further anodic shift in E_{fb} would initiate spontaneous OER by allowing electron transfer into the conduction band of Nb:$SrTiO_3$ and thus not reach equilibrium.

Careful examination of the carrier transport probed by cyclic voltammetry provides insight into the carrier dynamics in these heterostructures. At d_{LAO} < 1.5 u.c., E_{ON} shifts anodically, after which it reaches a plateau up to d_{LAO} = 2.0 u.c. similar to the E_{fb} trend. However, above d_{LAO} = 2.0 u.c., E_{ON} continues to shift anodically accompanied by a linear decrease in the photocurrent at fixed anodic bias (**Figure 3b**). The initial shift in E_{ON} and the reduction in the

oxidative photocurrent correspond well to the reduction in E_{fb}, reducing the electric field in the space charge layer in Nb:$SrTiO_3$, requiring additional potential to drive the photo-generated holes towards the surface. However, the behavior at d_{LAO} > 2.0 u.c. suggests the presence of effects independent from the dipole offset, most likely related to the materials specific properties of $LaAlO_3$ and its interface with $SrTiO_3$. The band gap of $LaAlO_3$ is 5.6 eV,[23] and its band edges are reported to be more negative than those of $SrTiO_3$, forming a staggered (type-II) heterojunction.[24] These band offsets can strongly impede the carrier transport as d_{LAO} increases, for example, by hole trapping at the $LaAlO_3$ valence band interfacing the cap $SrTiO_3$, or by recombination as they traverse across the cap $SrTiO_3$ with the electrons partially blocked by the cap $SrTiO_3$/$LaAlO_3$ conduction band offset. Furthermore, carrier trapping via intrinsic in-gap states inside the $LaAlO_3$ layer is expected to be enhanced as the carrier transit time increases with reduction in the built-in electric field at thicker d_{LAO}. Although disentangling each mechanism requires further investigation, the systematic evolution of photocurrent with d_{LAO} clearly indicates the fundamental impact of nm-thick dipole layers on the PEC performance of photoanodes.

In summary, we succeeded in shifting the flat band potential over 1.3 V by controllably inserting ~1 nm-thick subsurface dipole layers near the Nb:$SrTiO_3$ (001)/aqueous electrolyte interface. We emphasize that the flat band potential shift obtained in this study of 0.9 V per 0.4 nm of $LaAlO_3$ is significantly larger compared to any reported results in oxide/aqueous solution interfaces.[11] In addition to exploiting the strong ionicity of metal oxides, the atomic scale control of layered heterostructures allows spatial separation of the dipole layer from the oxide/solution interface. This minimizes deleterious specific adsorption which diminishes the dipole magnitude and the possibility of intercalation of ions at the surface, as often discussed in organic surface dipoles.[25,26] While the direction of the flat band potential shift was undesired for the

photoanodes in this study, application of this specific $LaAlO_3$ dipole layer to photocathodes should prove effective in increasing their performance. We also anticipate that a flat band potential shift in the opposite (cathodic) direction should be feasible by selecting an appropriate dipole layer. This study provides a proof-of-concept demonstration of a new approach to control the band edge alignments in an oxide epitaxial heterostructure that is structurally well-defined and well-characterized in solid-state Schottky junctions.[9] Given the large number of photoelectrodes previously studied, experimentally and theoretically, that have been classified as "unsuitable" due to the inappropriate band edge alignment,[3,27] the current results present a new strategy to revisit many of them to overcome their limitations by independently controlling the interface and the bulk properties to produce viable PEC devices.[28]

Experimental Section

Dipole engineered photoanode fabrication: All heterostructures were fabricated by pulsed laser deposition using a KrF excimer laser. The (001)-oriented single crystal Nb:$SrTiO_3$ substrates (Nb = 0.01 wt. %) were first pre-annealed under 950 ^{o}C for 30 minutes at partial oxygen pressure (P_{O2}) of 5×10^{-6} Torr to remove the carbon contaminants on the surface and to provide sharp atomic step-terrace structures. Subsequently, $LaAlO_3$ was grown at a growth temperature T_g = 800 ^{o}C and $P_{O2} = 1 \times 10^{-5}$ Torr, using a laser fluence of 0.61 J/cm^2 at a laser repetition rate of 1 Hz. The cap $SrTiO_3$ layer was deposited at T_g = 700 ^{o}C and $P_{O2} = 1 \times 10^{-6}$ Torr, under the laser fluence and repetition rate of 0.38 J/cm^2 and 1 Hz respectively. These samples were post-annealed at 1 atm of flowing oxygen at 450 ^{o}C for 1 hour to fill potential uncompensated oxygen vacancies generated during growth.

Photoelectrochemical characterization: PEC measurements were conducted in 0.1 M KOH solution using a Ag/AgCl 4M KCl reference electrode (Fisher Scientific, Accumet) and a coiled platinum wire counter electrode in the three-electrode setup. Experiments were conducted at

room temperature and the solution was continuously purged with oxygen gas. The Mott-Schottky plot was obtained by conducting electrochemical impedance spectroscopy between 10 kHz and 1 Hz at various DC potentials under dark conditions and was fit to the Randles model (Supporting Information Figure S2a) to extract the capacitance component in the electrode. For photocurrent measurements, a 1000 W xenon lamp provided concentrated broadband illumination. The power density of the utilizable photons (wavelength from 280 to 387 nm) was 3.70 mW/cm^2, which matches the power density of AM 1.5 G spectrum for the same wavelength range. Each sample has an exposed area of typically 0.03 cm^2, much smaller than the spot area from the light source. Cyclic voltammetry was obtained by sweeping the potential at 25 mV/s while chopping the light every 2 s.

Dipole engineered Schottky junction fabrication and characterization: The dipole engineered Pt/$LaAlO_3$/Nb:$SrTiO_3$ Schottky junctions were prepared by evaporating 5 nm thick platinum layer at 4×10^{-7} Torr using an e-beam evaporator at room temperature through a metal mask to form 400 μm-diameter metal electrodes. The built-in potential (V_{bi}) of these junctions were measured by capacitance-voltage technique using an LCR meter. V_{bi} was obtained by linearly fitting the $1/C^2$ data and extrapolating to the voltage axis. For $d_{LAO} > 1.0$ u.c., two linear fits were employed to account for the finite $1/C^2$ offset following the same procedure used in obtaining E_{fb} from electrochemical impedance measurements. Internal photoemission measurement was conducted by using a chopped monochromated tungsten-halogen lamp as the light source and a lock-in amplifier for detecting the photocurrent.

Supporting Information

Supporting Information is available from the Wiley Online Library or from the author.

Acknowledgements

This work was supported by the Department of Energy, Office of Basic Energy Sciences, Division of Materials Sciences and Engineering (heterostructure synthesis), and the Catalysis Science program within the Chemical Sciences, Geosciences, and Biosciences Division (PEC characterization), under contract DE-AC02-76SF00515. L.C.S. acknowledges support from the DARE Doctoral Fellowship supported by the Vice Provost for Graduate Education at Stanford University. P.C. acknowledges support from the Assistant Secretary for Energy Efficiency and Renewable Energy, Fuel Cell Technologies Office, of the U. S. Department of Energy.

Received: ((will be filled in by the editorial staff))
Revised: ((will be filled in by the editorial staff))
Published online: ((will be filled in by the editorial staff))

[1] a) N. S. Lewis and D. G. Nocera, *Proc. Natl. Acad. Sci. USA* **2009**, *103*, 15729; b) S. Chu and A. Majumdar, *Nature* **2012**, *488*, 294.

[2] J. M. Ogden, *Annu. Rev. Energy Environ.* **1999**, *24*, 227.

[3] A. Kudo and Y. Miseki, *Chem. Soc. Rev.* **2009**, *38*, 253.

[4] a) O. Khaselev and J. A. Turner, *Science* **1998**, *280*, 425; b) A. Kay, I. Cesar, M. Grätzel, *J. Am. Chem. Soc.* **2006**, *128*, 15714; c) A. Paracchino, V. Laporte, K. Sivula, M. Grätzel, E. Thimsen, *Nature Mater.* **2011**, *10*, 456; d) J. Su, L. Guo, N. Bao, C. A. Grimes, *Nano Lett.* **2011**, *11*, 1928; e) F. F. Abdi, L. Han, A. H. M. Smets, M. Zeman, B. Dam, R. Van de Krol, *Nature Commun.* **2013**, *4*, 2195.

[5] J. B. Goodenough, *Progr. Solid Stat. Chem.* **1971**, *5*, 145.

[6] a) H. Magnan, D. Stanescu, M. Rioult, E. Fonda, A. Barbier, *Appl. Phys. Lett.* **2012**, *101*, 133908; b) M. Seki, H. Yamahara, H. Tabata, *APEX* **2012**, *5*, 3; c) S. Kawasaki, R. Takahashi, K. Akagi, J. Yoshinobu, F. Komori, K. Horiba, H. Kumigashira, K. Iwashina, A. Kudo, M. Lippmaa, *J. Phys. Chem. C* **2014**, *118*, 20222.

[7] Y. Kozuka, Y. Hikita, C. Bell, H.Y. Hwang, *Appl. Phys. Lett.* **2010**, *97*, 012107.

[8] a) A. Ohtomo, D. A. Muller, J. L. Grazul, H. Y. Hwang, *Nature* **2002**, *419*, 378; b) M. Minohara, T. Tachikawa, Y. Nakanishi, Y. Hikita, L. F. Kourkoutis, J.-S. Lee, C.-C. Kao, M. Yoshita, H. Akiyama, C. Bell, H. Y. Hwang, *Nano Lett.* **2014**, *14*, 6743.

[9] T. Yajima, M. Minohara, C. Bell, H. Kumigashira, M. Oshima, H. Y. Hwang, Y. Hikita, *Nano Lett.* **2015**, *15*, 1622.

[10] a) J. W. Thackeray, M. J. Natan, P. Ng, M. S. Wrighton, *J. Am. Chem. Soc.* **1986**, *108*, 3570; b) C. M. Wang and T. E. Mallouk, *J. Phys. Chem.* **1990**, *94*, 423; c) C. M. Wang and T. E. Mallouk, *ibid.* **1990**, *94*, 4276; d) R. L.Grimm, M. J. Bierman, L. E. O'Leary, N. C. Strandwitz, B. S. Brunschwig, N. S. Lewis, *J. Phys. Chem. C* **2012**, *116*, 23569.

[11] a) F.-R. F. Fan and A. J. Bard, *J. Electrochem. Soc.* **1981**, *128*, 945; b) S. S. Kocha and J. A. Turner, *ibid.* **1995**, *142*, 2625; c) H. S. Hilal and J. A. Turner, *Electrochim. Acta* **2006**, *51*, 6487; d) Y.-S. Hu, A. Kleiman-Shwarsctein, G. D. Stucky, E. W. McFarland, *Chem. Commun.* **2009**, *19*, 2652; e) E. Johansson, S. W. Boettcher, L. E. O'Leary, A. D. Poletayev, S. Maldonado, B. S. Brunschwig, N. S. Lewis, *J. Phys. Chem. C* **2011**, *115*, 8594; f) F. Camacho-Alanis, H. Castaneda, G. Zangari, N. S. Swami, *Langmuir* **2011**, *27*, 11273; g) L. Xi, P. D. Tran, S. Y. Chiam, P. S. Bassi, W. F. Mak, H. K. Mulmudi, S. K. Batabyal, J. Barber, J. S. C. Loo, L. H. Wong, *J. Phys. Chem. C* **2012**, *116*, 13884; h) E. S. Brown, S. L. Peczonczyk, Z. Wang, S. Maldonado, *J. Phys. Chem. C* **2014**, *118*, 11593; i) B. A. MacLeod, K. X. Steirer, J. L. Young, U. Koldemir, A. Sellinger, J. A. Turner, T. G. Deutsch, D. C. Olson, *ACS Appl. Mater. Interfaces* **2015**, *7*, 11346; j) W. A. Smith, I. D. Sharp, N. C. Strandwitz, J. Bisquert, *Energy Environ. Sci.* **2015**, *8*, 2851.

[12] a) M. A. Butler and D. S. Ginley, *J. Electrochem. Soc.* **1978**, *125*, 228; b) V. Stevanovic, S. Lany, D. S. Ginley, W. Tumas, A. Zunger, *Phys. Chem. Chem. Phys.* **2014**, *16*, 3706.

[13] R. T. Tung, *Mat. Sci. Eng. R* **2001**, *35*, 1.

[14] a) Y. Hikita, M. Nishikawa, T. Yajima, H. Y. Hwang, *Phys. Rev. B* **2009**, *79*, 4; b) T. Yajima, Y. Hikita, M. Minohara, C. Bell, J. A. Mundy, L. F. Kourkoutis, D. A. Muller, H. Kumigashira, M. Oshima, H. Y. Hwang, *Nature Commun.* **2015**, *6*, 5.

[15] a) T. Watanabe, A. Fujishima, K. Honda, *Bull. Chem. Soc. Jpn.* **1976**, *49*, 355; b) M. S. Wrighton, A. B. Ellis, P. T. Wolczanski, D. L. Morse, H. B. Abrahamson, D. S. Ginley, *J. Am. Chem. Soc.* **1976**, *98*, 2774; c) J. Yin, J. H. Ye, Z. G. Zou, *Appl. Phys. Lett.* **2004**, *85*, 689.

[16] M. Kawasaki, K. Takahashi, T. Maeda, R. Tsuchiya, M. Shinohara, O. Ishiyama, T. Yonezawa, M. Yoshimoto, H. Koinuma, *Science* **1994**, *266*, 1540.

[17] a) N. Nakagawa, H. Y. Hwang, D. A. Muller, *Nature Mater.* **2006**, *5*, 204; b) S. Thiel, G. Hammerl, A. Schmehl, C. W. Schneider, J. Mannhart, *Science* **2006**, *313*, 1942.

[18] H. Gerischer, *Electrochim. Acta* **1989**, *34*, 1005.

[19] M. L. Reinle-Schmitt, C. Cancellieri, D. Li, D. Fontaine, M. Medarde, E. Pomjakushina, C. W. Schneider, S. Gariglio, P. Ghosez, J. M. Triscone, P. R. Willmott, *Nature Commun.* **2012**, *3*, 932.

[20] K. A. Müller and H. Burkard, *Phys. Rev. B* **1979**, *19*, 3593.

[21] a) R. De Gryse, W. P. Gomes, F. Cardon, and J. Vennik, *J. Electrochem. Soc*. **1975**, *122*, 711; b) M. Tomkiewicz, *J. Electrochem. Soc*. **1979**, *126*, 1505; c) C. C. L. McCrory, S. Jung, J. C. Peters, and T. F. Jaramillo, *J. Am. Chem. Soc*. **2013**, *135*, 16977.

[22] Y. Hikita, Y. Kozuka, T. Susaki, H. Takagi, and H. Y. Hwang, *Appl. Phys. Lett.* **2007**, *90*, 143507.

[23] S.-G. Lim, S. Kriventsov, T. N. Jackson, J. H. Haeni, D. G. Schlom, A. M. Balbashov, R. Uecker, P. Reiche, J. L. Freeouf, and G. Lucovsky, *J. Appl. Phys.* **2002**, *91*, 4500.

[24] G. Berner, A. Müller, F. Pfaff, J. Walde, C. Richter, J. Mannhart, S. Thiess, A. Gloskovskii, W. Drube, M. Sing, R. Claessen, *Phys. Rev. B* **2013**, *88*, 115111.

[25] a) S. Yang, D. Prendergast, J. B. Neaton, *Nano Lett.* **2012**, *12*, 383; b) J. B. Rivest, G. Li, I. D. Sharp, J. B. Neaton, D. J. Milliron, *J. Phys. Chem. Lett.* **2014**, *5*, 2450.

[26] a) J. A. Turner and B. A. Parkinson, *J. Electroanal. Chem.* **1983**, *150*, 611; b) L. A. Lyon, J. T. Hupp, *J. Phys. Chem.* **1995**, *99*, 15718.

[27] I. E. Castelli, T. Olsen, S. Datta, D. D. Landis, S. Dahl, K. S. Thygesen, K. W. Jacobsen, *Energy Environ. Sci.* **2012**, *5*, 5814.

[28] L. C. Seitz, Z. Chen, A. J. Forman, B. A. Pinaud, J. D. Benck, T. F. Jaramillo, *ChemSusChem* **2014**, *7*, 1372.

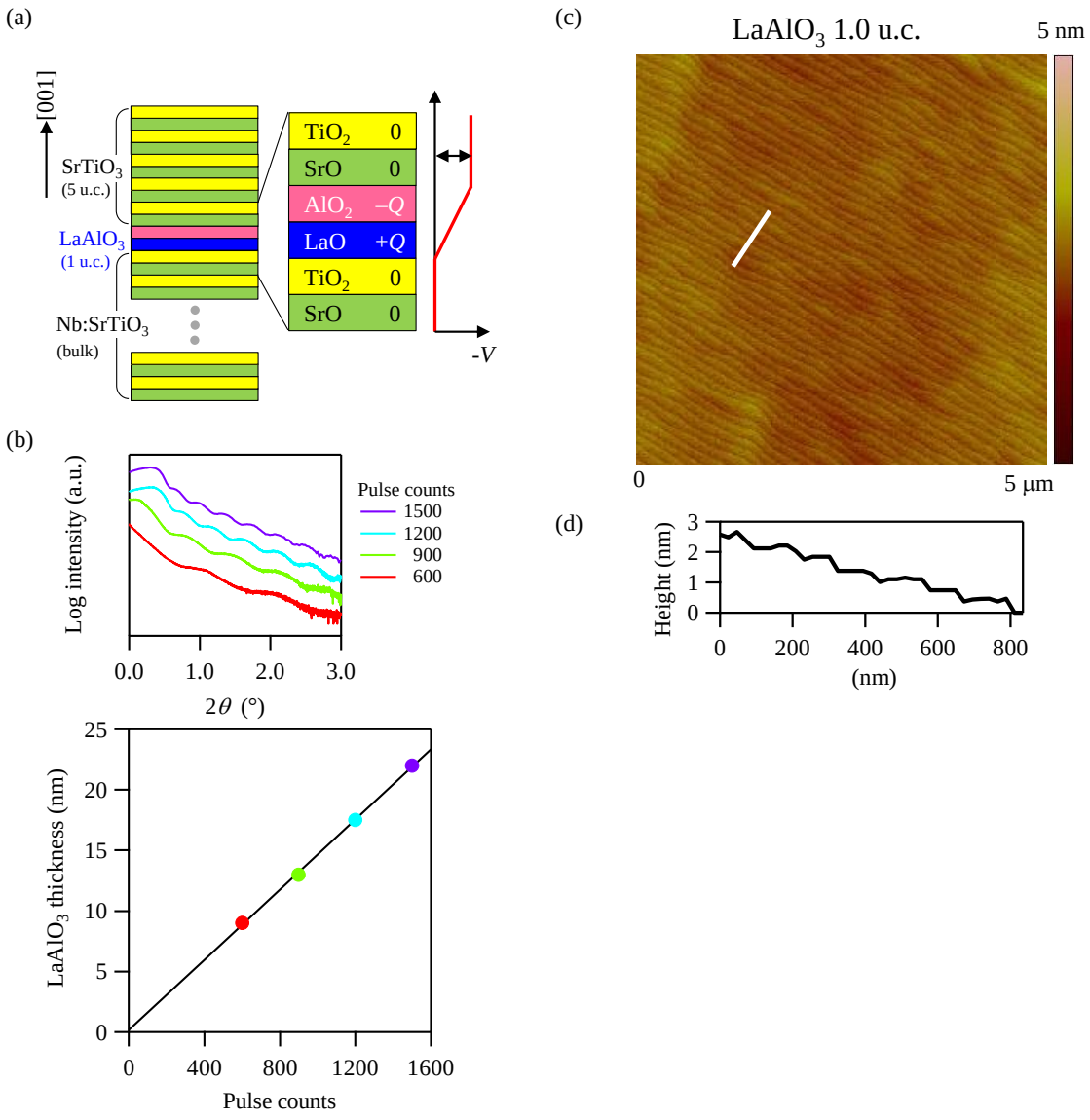

Figure 1. (a) Schematic of the dipole engineered Nb:$SrTiO_3$ photoelectrode employed in this study. -*V* corresponds to the dipole potential offset. (b) X-ray reflectivity data of $LaAlO_3$/$SrTiO_3$ (001) heterostructures with varying the laser pulse counts (top) and the extracted $LaAlO_3$ layer thickness (bottom). (c) AFM topography of the d_{LAO} = 1.0 u.c. sample surface showing a particle free step-terrace structure. (d) Lateral scan across the white line in (c) presenting 0.4 nm step heights corresponding to single perovskite unit cells.

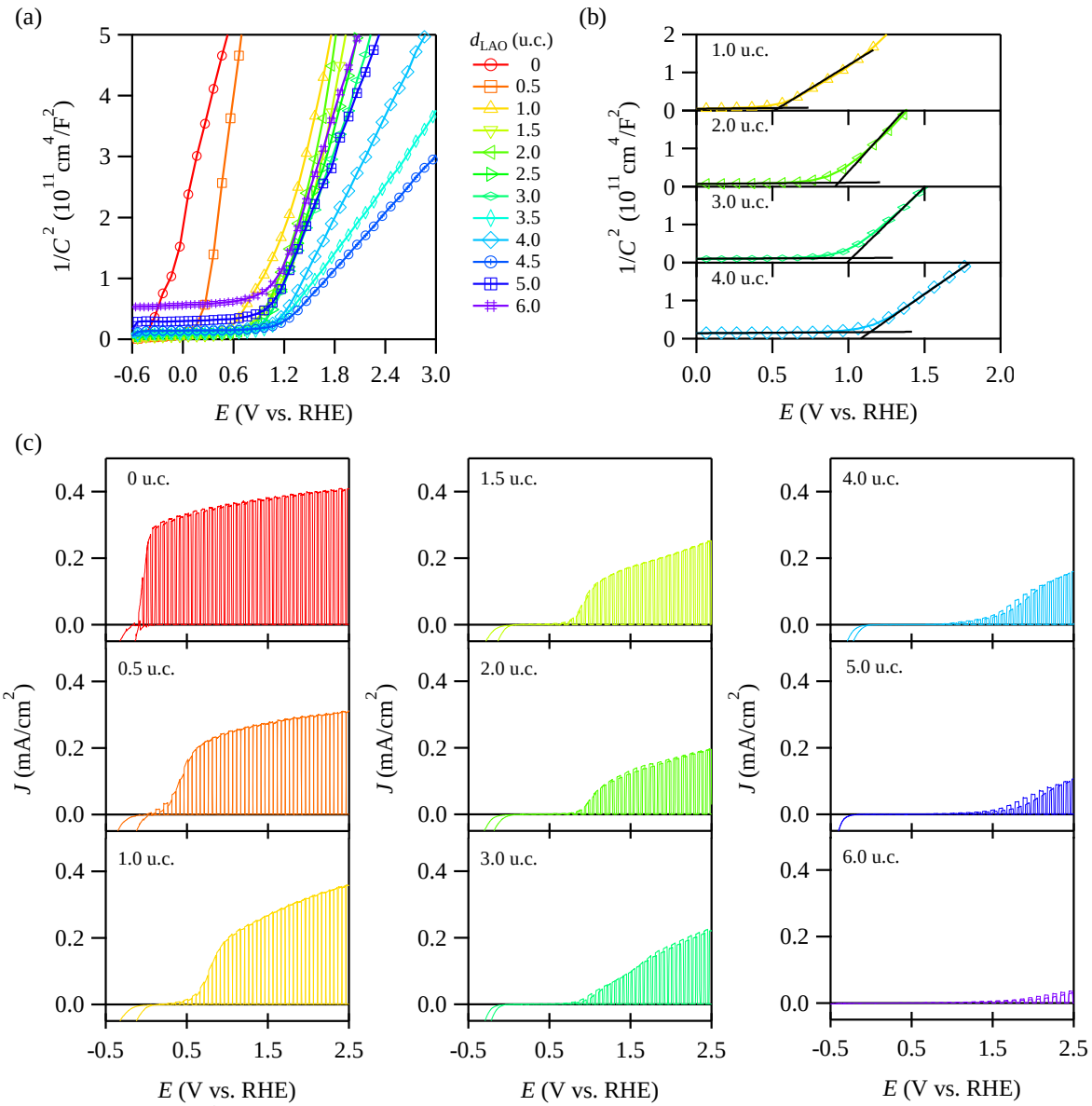

Figure 2. (a) $1/C^2 - E$ plot for the 12 samples with different d_{LAO}. (b) Magnified plot for d_{LAO} = 1.0, 2.0, 3.0, and 4.0 u.c. showing the deduction of E_{fb} from two linear fits to the $1/C^2 - E$ data. (c) Cyclic voltammetry curves for 9 dipole engineered photoanodes under 2 s chopped white light irradiation. The number in each panel indicates the $LaAlO_3$ dipole layer thickness d_{LAO}.

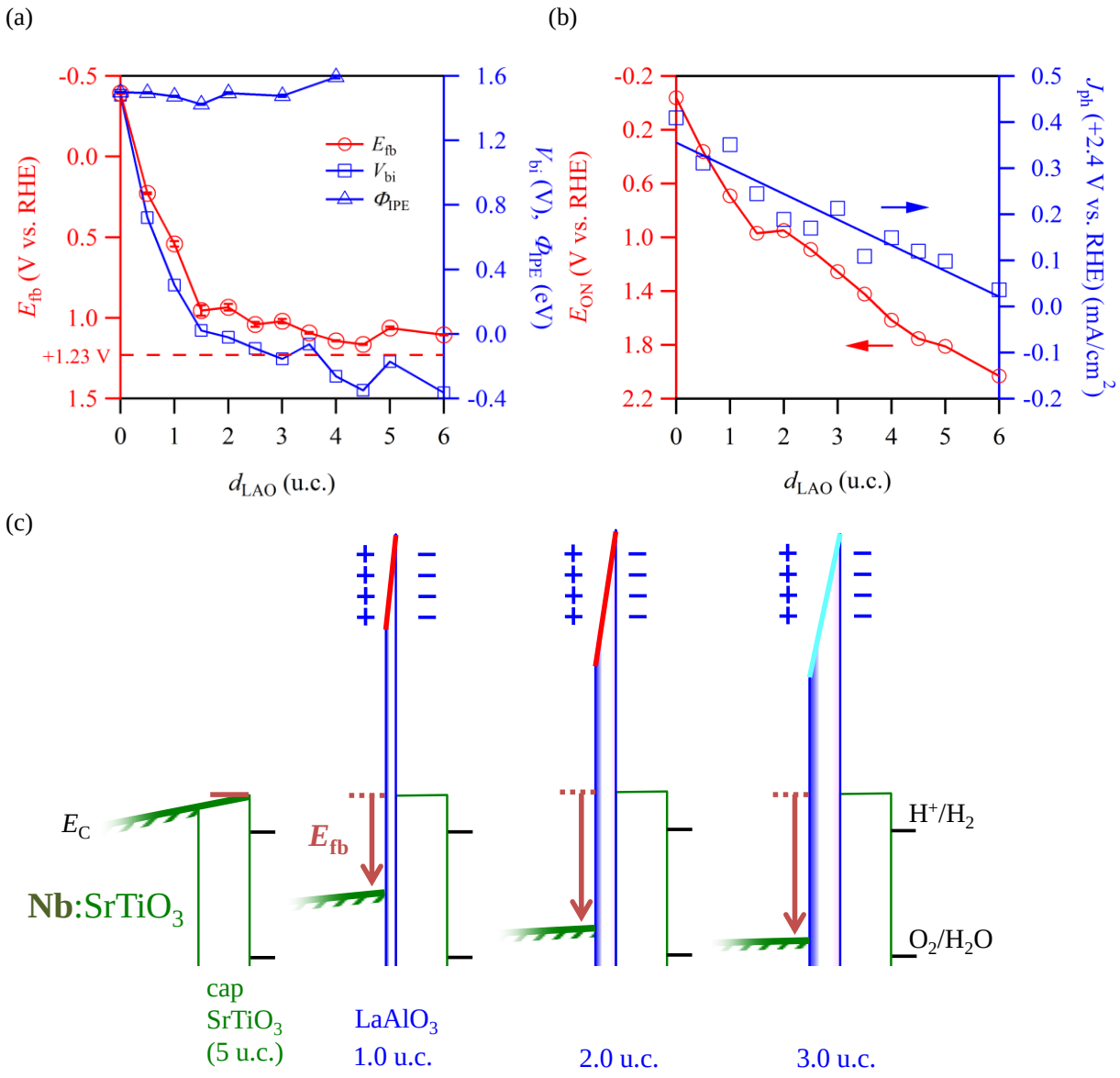

Figure 3. (a) E_{fb} (red, left) in solution from the Mott-Schottky analysis and V_{bi} and Φ_{IPE} (blue, right) from Pt-Schottky junction measurements plotted against d_{LAO}. The horizontal dotted line indicates the oxygen evolution potential E_{OER}. (b) E_{ON} (red, left) and J_{ph} at E = +2.4 V vs. RHE (blue, right) plotted as a function of d_{LAO}. (c) Schematic interface band diagram showing the evolution of E_{fb} in $SrTiO_3$ (5 u.c.)/$LaAlO_3$ (d_{LAO})/Nb:$SrTiO_3$ (001) heterostructures.

Flat band potential at an oxide semiconductor/aqueous electrolyte interface was systematically shifted over 1.3 V by atomically engineering an electrostatic dipole layer near this interface. Coherent stacking of polar oxide surfaces stabilizes a large internal electric field over atomic distances. This technique enables the decoupling of the bulk and interface constraints in designing photoelectrodes using complex oxides.

Band edge engineering of oxide photoanodes for photoelectrochemical water splitting: Integration of subsurface dipoles with atomic-scale control

Yasuyuki Hikita, Kazunori Nishio, Linsey C. Seitz, Pongkarn Chakthranont, Takashi Tachikawa, Thomas F. Jaramillo, Harold Y. Hwang*

Keyword

interface dipoles, oxide/electrolyte interfaces, photoelectrochemical cells, solar water splitting, $SrTiO_3$